HMI Data Driven MHD Model Predicted Active Region Photospheric Heating Rates: Their Scale Invariant Power Law Distributions, and Their Plausible Temporal Correlation With Flares

Michael L. Goodman - Jacobs ESSSA/NASA Marshall Space Flight Center
michael.l.goodman@nasa.gov

Chiman Kwan, Bulent Ayhan & Eric L. Shang - Applied Research LLC

Work Partially Supported by a NASA Phase 1 SBIR Award

JACOBS
ESSSA Group

1. Introduction & Summary of Approach and Results

- **Flare forecasting is important for protecting astronauts and space assets.**
- **How can forecasting be improved?**
- **Flares involve the largest current densities in the solar atmosphere.**
- **The magnetic field B, and hence current density $\mathbf{J} = c\nabla \times \mathbf{B}/(4\pi)$ are most accurately known at the photosphere.**
- **Large flares (M, X) occur in the neutral line regions (NLRs) of active regions (ARs). J is max. in NLRs. $B_{vertical}$ changes sign. Max. free energy.**
- **Are there changes in the photospheric J in NLRs of ARs that are useful for forecasting M/X flares?**
- **Can HMI (Helioseismic & Magnetic Imager) be used to detect previously undetected changes in J?**

- **HMI: Full disk, continuous time observations of photospheric B at $1''$, 12 minute resolution. High enough to begin to resolve granulation dynamics: space and time scales ~ 1000 km and $\sim 15-20$ minutes.**

- **Existing flare models we are aware of do not compute the complete J. $\mathbf{J} \neq 0 \Leftrightarrow$ non-potential B. Flares relax B towards $\mathbf{J} = \mathbf{0}$: Min. energy state.**

- **Objective: Develop a model that computes J using highest resolution data with continuous space and time coverage of entire ARs.**

- **Problem: Photospheric measurements return $\mathbf{B}(x, y, t)$, not $\mathbf{B}(x, y, z, t)$. So J_z can be computed, but not J_x or J_y.**

- **Solution: We combine HMI data, the $\nabla \cdot \mathbf{B} = 0$ constraint, and a Fourier expansion of B in (x, y) to determine $\mathbf{B}(x, y, z, t)$ through second order in z, where $z = 0$ is the photosphere.**

- **Then the complete $\mathbf{J}(x, y, 0, t)$ can be computed.**

- **From B(x, y, z, t) compute $\mathbf{J}, \mathbf{A}, \mathbf{E}$ in each pixel for 14 ARs. 7 with M/X flares. 7 with B, C, or no flares.**

- **Compute time series of $Q(t) = \eta J^2$ for each AR NLR(t). Are there correlations between changes in Q and M/X flare times?**

  Answer: Plausibly yes.

- **Compute the cumulative distribution function (CDF) $N(Q)$ for each AR time series of Q. $N(Q)$ is the number of events with heating rates $\geq Q$. Compare with the observed $N(E)$ for the total energy E released in solar flares. E is the amount of magnetic energy converted into particle energy.**

  Result: Like $N(E)$, $N(Q)$ is a scale invariant power law distribution: $N(Q) = C_{AR} Q^{-S}$. $N(Q)$ and $N(E)$ have essentially the same exponent range.

2. Magnetic Field

Let L_x and L_y be the x and y dimensions of the rectangular region used to enclose most or all of the AR modeled. The HMI pixel side length $\Delta = 0.5''$. The number of HMI data points covering this region is $N = (N_x + 1)(N_y + 1)$, where $N_x = L_x/\Delta, N_y = L_y/\Delta$, and (N_x, N_y) are given by the HMI datasets. For sufficiently small z,

$$\mathbf{B}(x, y, z, t) = e^{-z/L(x,y,t)} \sum_{n=0}^{N_x} \sum_{m=0}^{N_y} \mathbf{b}_{nm}(t) e^{2\pi i\left(\frac{nx}{L_x} + \frac{my}{L_y}\right)}. \tag{1}$$

- **$\mathbf{b}_{nm}(t)$ are complex, and $L(x, y, t) = L_0(x, y, t) + zL_1(x, y, t)/L_0$ where L_0 and L_1 are real and determined by the HMI data and the $\nabla \cdot \mathbf{B} = 0$ condition.**
- **For $z = 0$, and given the N vectors $\mathbf{B}(x_i, y_i, 0, t_j)$ from the HMI data for each j, Eq. (1) is solved for the time series of the $\mathbf{b}_{nm}(t)$ using a FFT.**

2.1. The $\nabla \cdot \mathbf{B} = 0$ Condition

Define $\mathbf{B}_0 = \mathbf{B}(x, y, 0, t)$. Take the divergence of Eq. (1) and set it equal to zero. Solving the resulting equation through order z gives

$$L_0(x, y, t) = \frac{B_{0z}}{B_{0x,x} + B_{0y,y}}, \tag{2}$$

and

$$L_1(x, y, t) = -\frac{L_0}{2B_{0z}} \left(B_{0x} L_{0,x} + B_{0y} L_{0,y} \right). \tag{3}$$

The right hand sides of Eqs. (2) and (3) are evaluated at $z = 0$. Therefore, L_0 and L_1 are completely determined by the HMI data. Gives $\partial \mathbf{B}/\partial z$ at $z = 0$.

It is the $\nabla \cdot \mathbf{B} = 0$ condition plus the HMI data that determine the z dependence of the model that allows J_x and J_y to be computed.

3. Current Density

The current density $\mathbf{J}(x,y,z,t) = c\nabla\times\mathbf{B}/(4\pi)$**. Through order** z**,**

$$
\begin{aligned}
(\nabla\times\mathbf{B})_x &= \exp(-z/L)\left[\frac{z}{L_0^2}L_{0,y}B_{0z} + B_{0z,y} + \frac{1}{L_0}\left(1-\frac{2L_1z}{L_0^2}\right)B_{0y}\right], & (4)\\
(\nabla\times\mathbf{B})_y &= -\exp(-z/L)\left[\frac{z}{L_0^2}L_{0,x}B_{0z} + B_{0z,x} + \frac{1}{L_0}\left(1-\frac{2L_1z}{L_0^2}\right)B_{0x}\right], & (5)\\
(\nabla\times\mathbf{B})_z &= \exp(-z/L)\left[\frac{z}{L_0^2}\left(L_{0,x}B_{0y} - L_{0,y}B_{0x}\right) + \left(B_{0y,x} - B_{0x,y}\right)\right]. & (6)
\end{aligned}
$$

4. Vector Potential and Electric Field

Assume the following expansion, valid through order z^3 for sufficiently small z.

$$\mathbf{A}(x, y, z, t) = \mathbf{a}_0(x, y, t) + \mathbf{a}_1(x, y, t)z + \mathbf{a}_2(x, y, t)z^2 + \mathbf{a}_3(x, y, t)z^3. \tag{7}$$

Expand B through order z^2 to obtain

$$\mathbf{B}(x, y, z, t) = \left(1 - \frac{z}{L_0} + \left(1 + \frac{2L_1}{L_0}\right)\frac{z^2}{2L_0^2}\right)\mathbf{B}_0(x, y, t) \tag{8}$$

- **The $\mathbf{a}_i (0 \leq i \leq 3)$ are found by solving $\mathbf{A} = \nabla \times \mathbf{B}$ with the Coulomb gauge condition $\nabla \cdot \mathbf{A} = 0$ (ensures uniqueness), order by order in powers of z.**

Let Σ' denote the sum over n, m except the term with $n = m = 0$. Then

$$\begin{aligned} A_x &= -\frac{L_x^2 L_y}{2\pi}\sum{}' \frac{m I_{z,nm}}{\left(n^2 L_y^2 + m^2 L_x^2\right)} - \frac{y R_{z,00}}{2} + z\left(1 - \frac{z}{2L_0}\right) B_{0y} + \\ &\quad \frac{1}{6}\left(\left(1 + \frac{2L_1}{L_0}\right)\frac{B_{0y}}{L_0^2} - \left(B_{0y,xx} - B_{0x,xy}\right)\right) z^3 \qquad (9) \\ A_y &= \frac{L_x L_y^2}{2\pi}\sum{}' \frac{n I_{z,nm}}{\left(n^2 L_y^2 + m^2 L_x^2\right)} + \frac{x R_{z,00}}{2} - z\left(1 - \frac{z}{2L_0}\right) B_{0x} - \\ &\quad \frac{1}{6}\left(\left(1 + \frac{2L_1}{L_0}\right)\frac{B_{0x}}{L_0^2} - \left(B_{0x,yy} - B_{0y,xy}\right)\right) z^3 \qquad (10) \\ A_z &= \left[-\frac{1}{2}\left(B_{0y,x} - B_{0x,y}\right)\left(1 - \frac{z}{3L_0}\right) + \frac{z}{6L_0^2}\left(B_{0x}L_{0,y} - B_{0y}L_{0,x}\right)\right] z^2. \qquad (11) \end{aligned}$$

Then $\mathbf{E} = -c^{-1}\partial\mathbf{A}/\partial t - \nabla\Phi \sim -c^{-1}\partial\mathbf{A}/\partial t$.

5. Need to Remove Spurious Doppler Periods From the HMI B

- **There is spurious, Doppler shift generated noise in the form of 6, 12, and 24 hour period oscillations in the components of B for each pixel. Noise is due to SDO orbital motion.**

- **The noise is removed from the time series of HMI B for each pixel using an FFT based bandpass filter.**

- **Doppler Noise in Pixel Level Quantities:**

  Figures 1-3 shows the filtered and un-filtered HMI time series of B_x, B_y, and B_z for a randomly selected pixel from the NLR of NOAA AR 1166 during a 70 hour long time series.

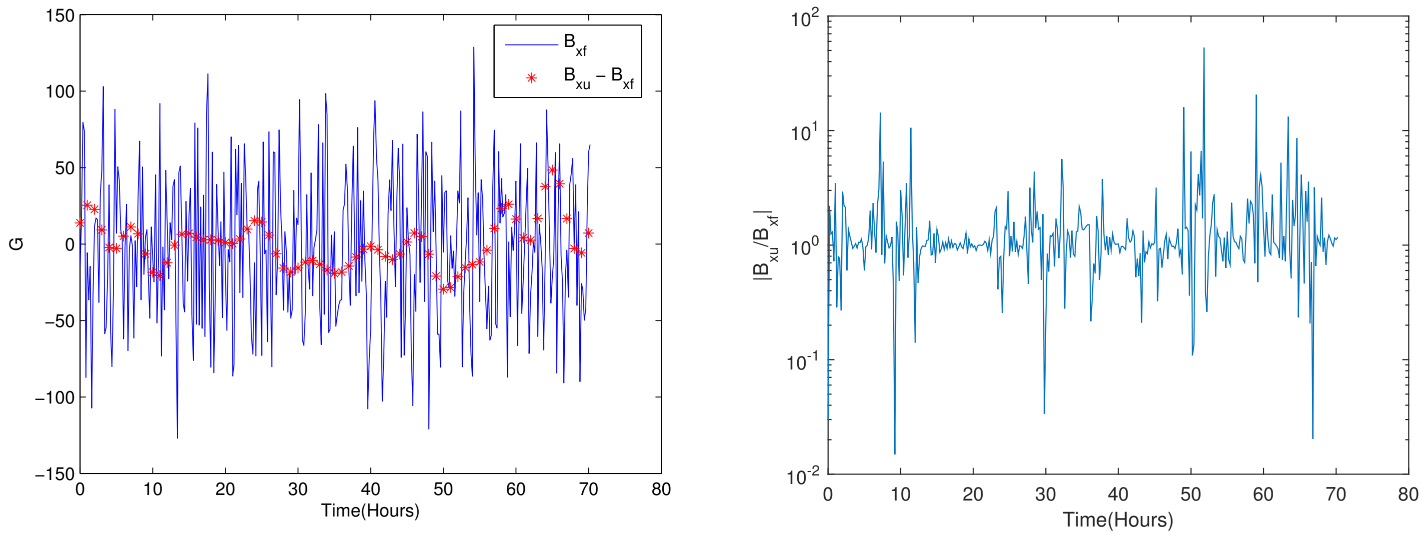

Figure 1: Comparison of the Filtered and Un-filtered B_x in a pixel from NLR/AR 1166.

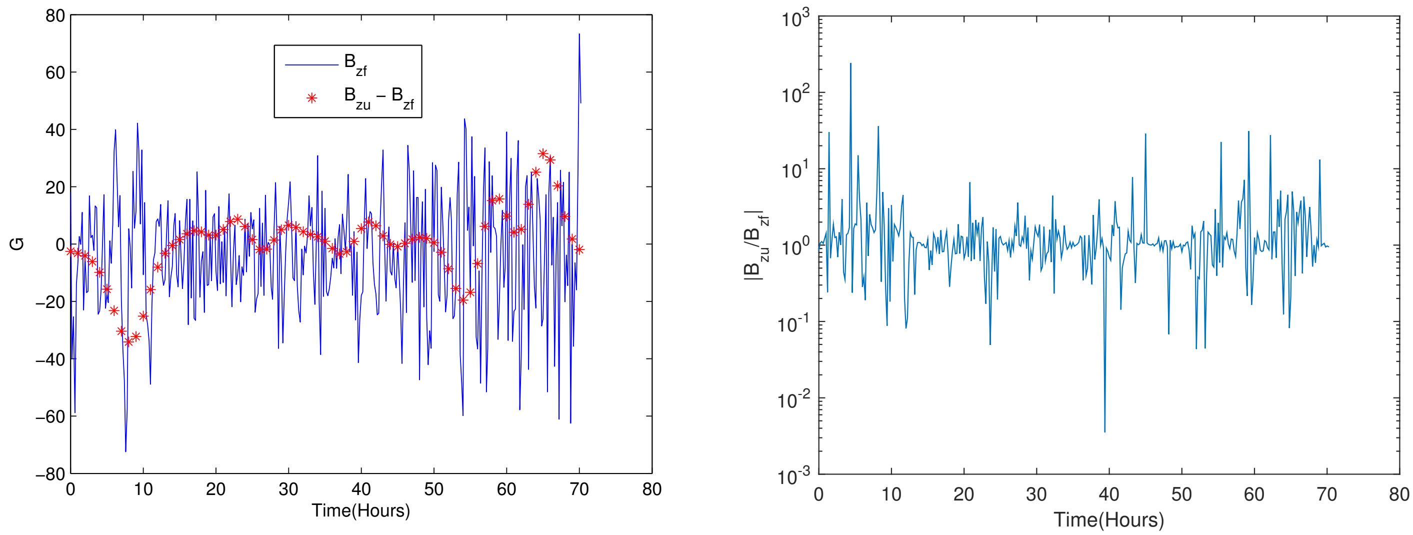

Figure 2: Comparison of the Filtered and Un-filtered B_z in a pixel from NLR/AR 1166.

- **Doppler Noise in NLR Integrated Quantities:**

  Figures 4-7 show the results of integrating the filtered and un-filtered pixel level results for ηJ^2 and $B^2/8\pi$ over the NLR at each time.

  The 70 hour long time interval includes 1 X, 2 M, and 9 C flares.

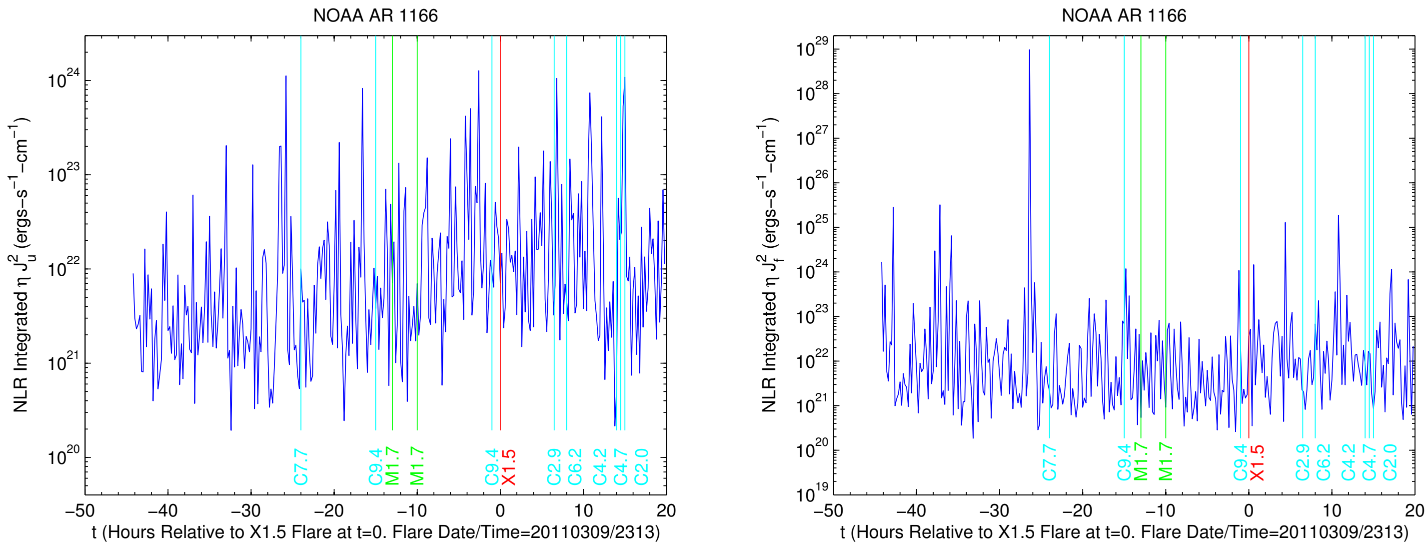

Figure 3: Comparison of the filtered and un-filtered, NLR integrated ηJ^2.

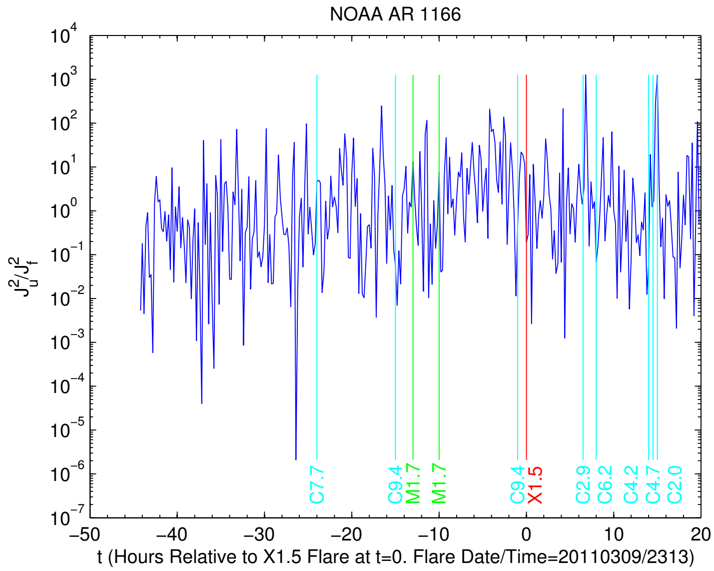

Figure 4: Comparison of the filtered and un-filtered, NLR integrated ηJ^2.

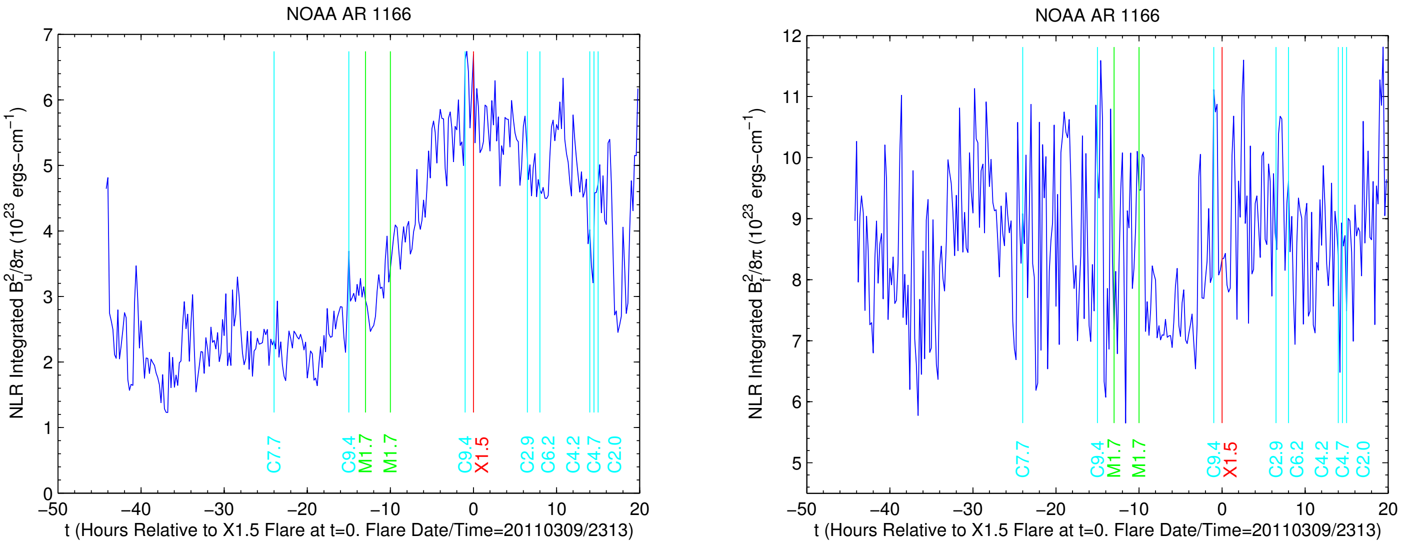

Figure 5: Comparison of the filtered and un-filtered, NLR integrated $B^2/8\pi$.

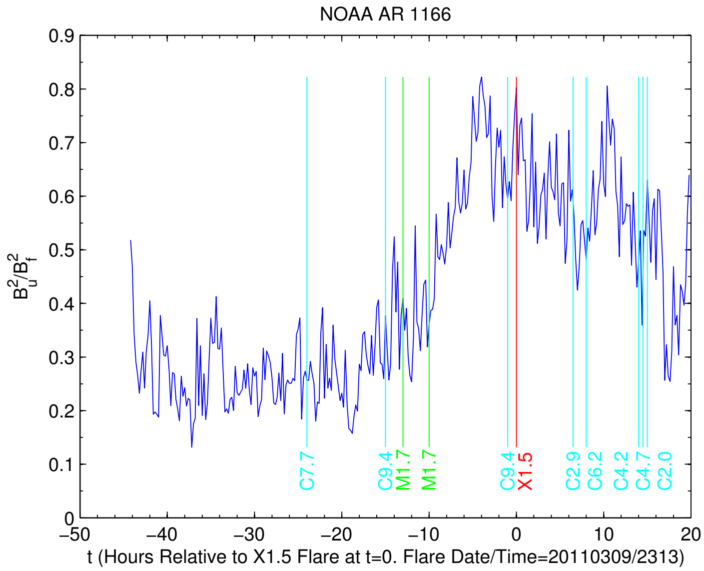

Figure 6: Comparison of the filtered and un-filtered, NLR integrated $B^2/8\pi$.

6. NLR Integrated Resistive Heating Rates $Q(t)$ of Strongly Flaring (SF) ARs: Comparison with Flare Times

- **Plot $Q(t)$. Superimpose the times of C, M, and X flares. NOAA database.**
- **Look for changes in Q that may be correlated with flare times. Large spikes.**
- **Check to what extent J is force-free (i.e. $J_{\perp}/J_{\parallel} \ll 1$). The largest heating events, which are found to occur in single pixels, are highly non-force-free: $\mathbf{J} \times \mathbf{B} = 0$ is a bad assumption at the photosphere.**
- **Results for weakly flaring ARs (C, B, or no flares) are not shown. Q is $\sim 10 - 100$ times less than for SF ARs, and there does not seem to be a correlation between spikes in Q and subsequent flaring.**

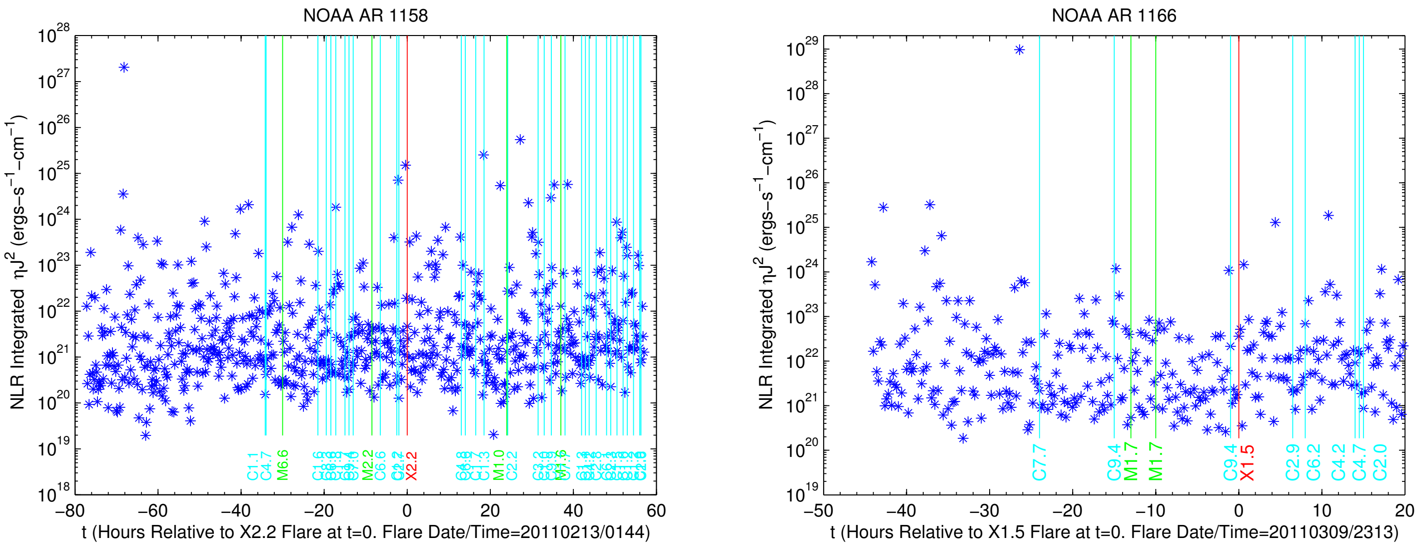

Figure 7: NLR integrated Q for 2 of 7 SF ARs.

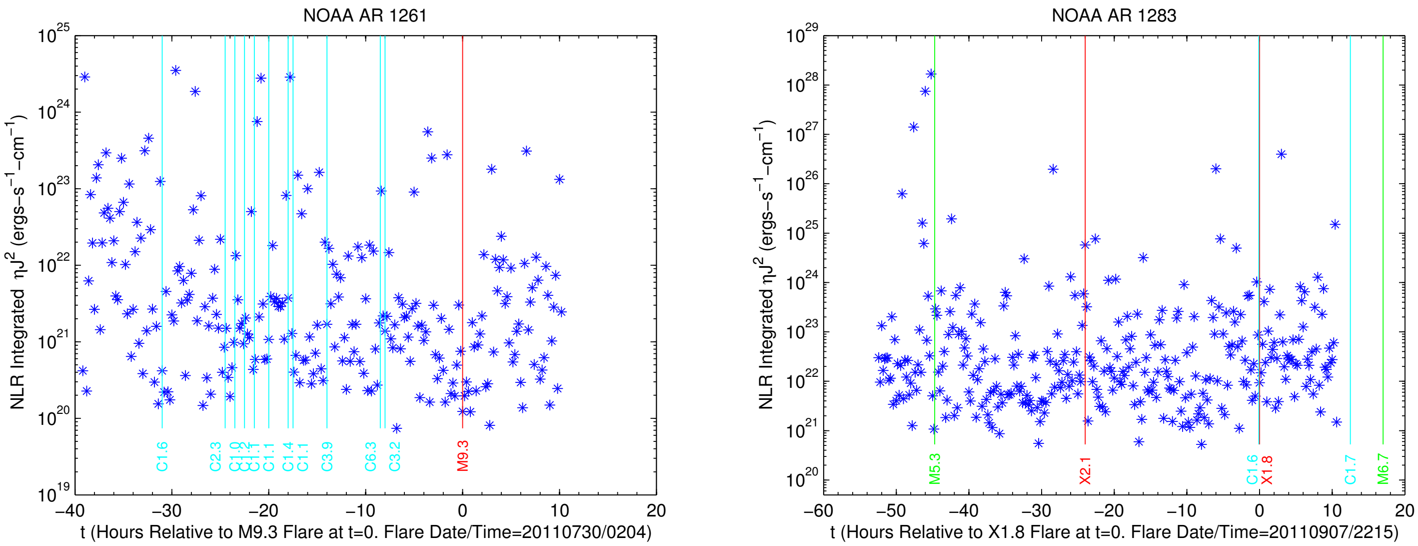

Figure 8: NLR integrated Q for 2 of 7 SF ARs.

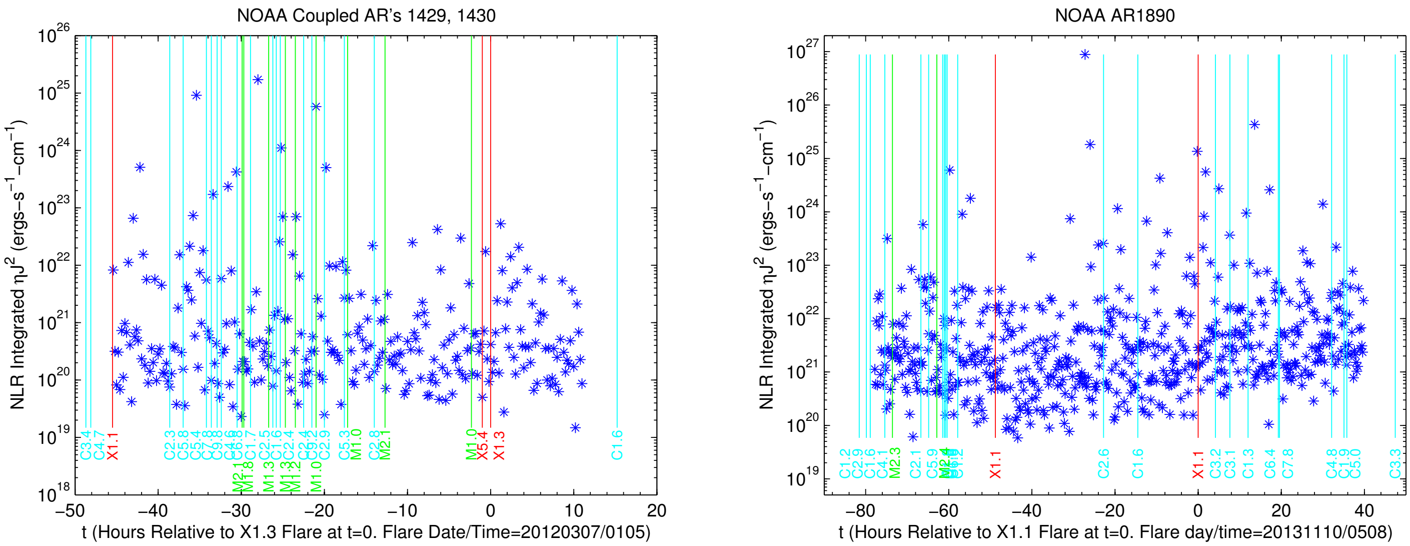

Figure 9: NLR integrated Q for 2 of 7 SF ARs.

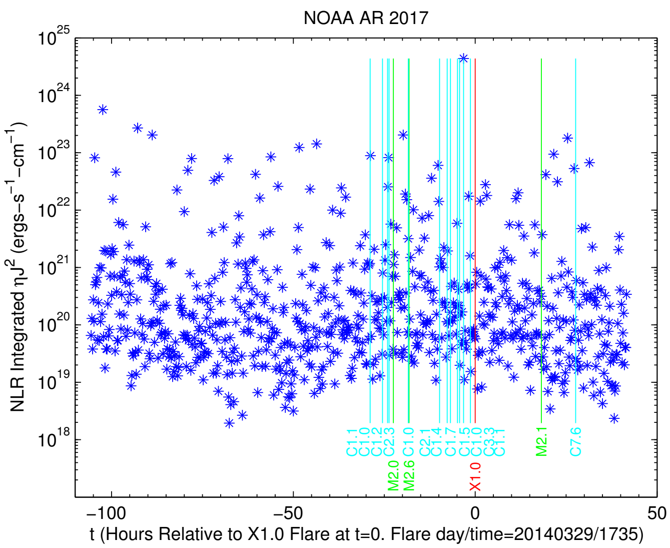

Figure 10: NLR integrated Q for the 7th SF AR.

7. Scale Invariant Power Law Distributions of Q - Comparison with Flares

- **Compute the Cumulative Distribution Functions (CDFs) of the time series for Q. The CDF is the number $N(Q)$ of heating events with heating rate $\geq Q$.**

- **Above an AR dependent threshold value, the CDF for each AR is well fit by a scale invariant power law distribution $N(Q) = AQ^{-S}$, with S constant over a range of several orders of magnitude in Q.**

  Scale invariance means that a change in scale of Q (i.e. replacing Q by kQ) does not change the form of $N(Q)$ (i.e. $N(kQ) =$ constant $\times N(Q)$). $N(Q)$ is scale invariant over the range of Q for which S is constant.

- **For the 14 ARs analyzed it is found that $0.40 \leq S \leq 0.53$, with a mean and standard deviation across the ARs of 0.47 and 0.045. This $\Rightarrow$ little statistical variation in S from one AR to another.**

- **The CDF $N(E)$ for the total energy E released in solar flares is determined from observations to have the same form: $N(E) =$ constant $\times E^{-\alpha}$.**

- **EUV and SXR observations of nanoflares in the $0.7-4$ MK range, and HXR observations of flares imply that $0.51 \leq \alpha \leq 0.57$, and $0.4 \leq \alpha \leq 0.6$.**

- **Observations also show that, as is found for the exponent S in $N(Q)$, there is little variation of α among ARs.**

- **Therefore, the power law scaling of the *photospheric* Q is essentially identical to that found for *coronal* flares.**

- **Suggests the mechanisms that generate Q and coronal flares are closely related.**

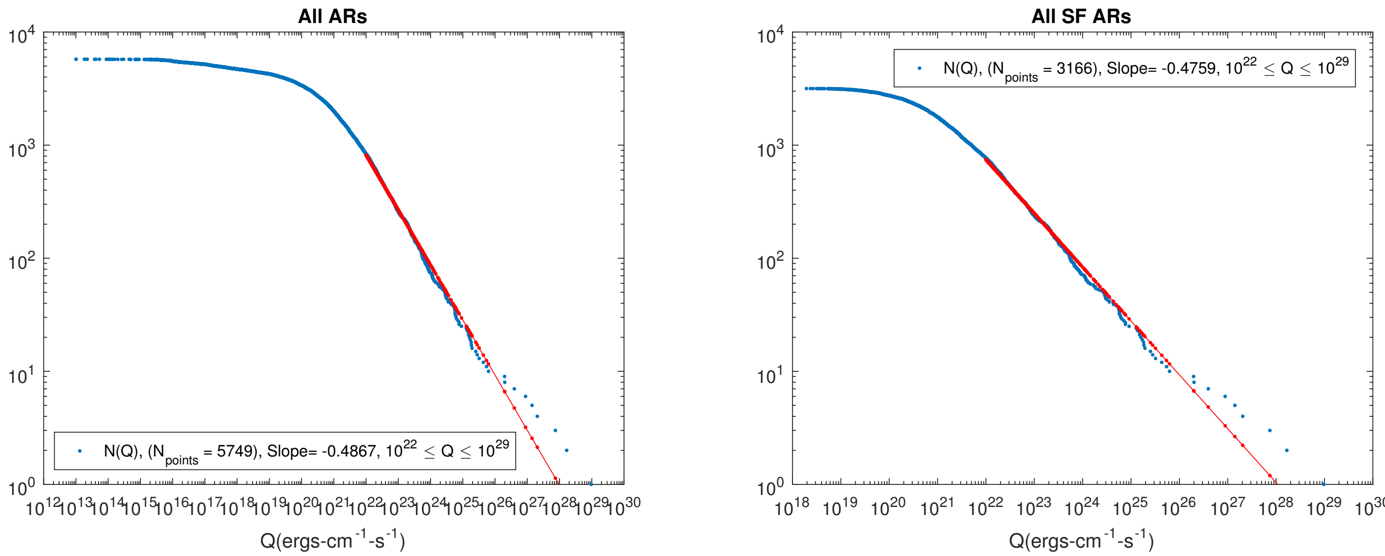

Figure 11: CDFs for all ARs, and all SF ARs.

8. Conclusions

- **Flare forecasting models based on computing time dependent maps of the complete photospheric current density need to be developed.**

- **The spurious Doppler periods in the HMI magnetic field can introduce large errors into B and derived quantities.**

- **In combination with the model, HMI might be revealing previously undetected photospheric heating events on granulation space and time scales in NLRs of ARs.**

- **The largest heating events occur in NLRs that exhibit M/X flares. They are highly non-force-free.**

- **It is plausible these events are correlated with M/X flares, preceding them by several hours to several days. But the sample size of 14 ARs is too small to determine if a correlation exists. Analysis of more ARs is needed.**

- **The CDFs of Q obey a scale invariant power law distribution essentially identical to that of the energy released in flares. This suggests a close connection between the process that drives Q, which is a photospheric phenomenon, and the process that drives flares, which are a coronal phenomenon.**